# Spatial distributions of white matter hyperintensities on brain MRI: A pooled analysis of individual participant data from 11 memory clinic cohorts

Mirthe Coenen [a,*], Geert Jan Biessels [a], Charles DeCarli [b], Evan F. Fletcher [b], Pauline M. Maillard [b], Alzheimer's Disease Neuroimaging Initiative [1], Frederik Barkhof [c,d], Josephine Barnes [e], Thomas Benke [f], Jooske M.F. Boomsma [g], Christopher P.L.H. Chen [h,i], Peter Dal-Bianco [j], Anna Dewenter [k], Marco Duering [k,l], Christian Enzinger [m,n], Michael Ewers [k], Lieza G. Exalto [a], Nicolai Franzmeier [k,o,p], Onno Groeneveld [a,q], Saima Hilal [h,i,r], Edith Hofer [s,t], Huiberdina L. Koek [u], Andrea B. Maier [i,v,w,x], Cheryl R. McCreary [x], Janne M. Papma [y,z], Ross W. Paterson [e], Yolande A.L. Pijnenburg [g], Anna Rubinski [k], Reinhold Schmidt [s], Jonathan M. Schott [e], Catherine F. Slattery [e], Eric E. Smith [x], Carole H. Sudre [aa,ab,ac], Rebecca M.E. Steketee [y,ad], Esther van den Berg [y,z], Wiesje M. van der Flier [g], Narayanaswamy Venketasubramanian [i,ae], Meike W. Vernooij [y,ad,af], Frank J. Wolters [y,ad,af], Xu Xin [h,i], J. Matthijs Biesbroek [a,ag], Hugo J. Kuijf [ah]

[a] *Department of Neurology and Neurosurgery, UMC Utrecht Brain Center, Utrecht, the Netherlands*
[b] *Department of Neurology, University of California at Davis, USA*
[c] *Radiology & Nuclear Medicine, Amsterdam UMC, Location Vrije Universiteit, the Netherlands*
[d] *UCL Institute of Neurology, London, UK*
[e] *Dementia Research Centre, UCL Queen Square Institute of Neurology, UCL, London, UK*
[f] *Clinic of Neurology, Medical University Innsbruck, Austria*
[g] *Alzheimer Center Amsterdam, Department of Neurology, Amsterdam Neuroscience, Vrije Universiteit Amsterdam, Amsterdam UMC, Amsterdam, the Netherlands*
[h] *Department of Pharmacology, National University of Singapore, Singapore, Singapore*
[i] *Memory, Aging and Cognition Center, National University Health System, Singapore, Singapore*
[j] *Department of Neurology, Medical University Vienna, Austria*
[k] *Institute for Stroke and Dementia Research (ISD), University Hospital, LMU Munich, Munich, Germany*
[l] *Medical Image Analysis Center (MIAC) and Department of Biomedical Engineering, University of Basel, Basel, Switzerland*
[m] *Division of General Neurology, Department of Neurology, Medical University Graz, Austria*
[n] *Division of Neuroradiology, Interventional and Vascular Radiology, Department of Radiology, Medical University of Graz, Austria*
[o] *Department of Psychiatry and Neurochemistry, Institute of Neuroscience and Physiology, The Sahlgrenska Academy, University of Gothenburg, Gothenburg, Sweden*
[p] *Munich Cluster for Systems Neurology (SyNergy), Munich, Germany*
[q] *Department of Neurology, Isala, Meppel, the Netherlands*
[r] *Saw Swee Hock School of Public Health, National University of Singapore and National University Health System, Singapore, Singapore*
[s] *Division of Neurogeriatrics, Department of Neurology, Medical University of Graz, Austria*
[t] *Institute for Medical Informatics, Statistics and Documentation, Medical University of Graz, Austria*
[u] *Department of Geriatric Medicine, University Medical Center Utrecht, Utrecht, the Netherlands*
[v] *Healthy Longevity Translational Research Programme, Yong Loo Lin School of Medicine, National University of Singapore, Singapore*
[w] *Centre for Healthy Longevity, @AgeSingapore, National University Health System, Singapore*
[x] *Department of Clinical Neurosciences and Radiology and Hotchkiss Brain Institute, University of Calgary, Calgary, Alberta, Canada*
[y] *Alzheimer Center Erasmus MC, Erasmus MC University Medical Center, Rotterdam, the Netherlands*
[z] *Department of Neurology, Erasmus MC University Medical Center, Rotterdam, the Netherlands*
[aa] *MRC Unit for Lifelong Health and Ageing at UCL, University College London, London, UK*
[ab] *Centre for Medical Image Computing, Department of Computer Science, University College London, London, UK*

* Corresponding author at: University Medical Center Utrecht, PO-Box: 85500, ZIP code: 3508 GA, The Netherlands.
*E-mail address:* m.coenen@umcutrecht.nl (M. Coenen).

ac *School of Biomedical Engineering & Imaging Sciences, King's College London, London, UK*
ad *Department of Radiology & Nuclear Medicine, Erasmus MC University Medical Center, Rotterdam, the Netherlands*
ae *Raffles Neuroscience Center, Raffles Hospital, Singapore, Singapore*
af *Department of Epidemiology, Erasmus MC University Medical Center, Rotterdam, the Netherlands*
ag *Department of Neurology, Diakonessenhuis Hospital, Utrecht, the Netherlands*
ah *Image Sciences Institute, University Medical Center Utrecht, Utrecht, the Netherlands*

---

## ARTICLE INFO

## ABSTRACT

*Introduction:* The spatial distribution of white matter hyperintensities (WMH) on MRI is often considered in the diagnostic evaluation of patients with cognitive problems. In some patients, clinicians may classify WMH patterns as "unusual", but this is largely based on expert opinion, because detailed quantitative information about WMH distribution frequencies in a memory clinic setting is lacking. Here we report voxel wise 3D WMH distribution frequencies in a large multicenter dataset and also aimed to identify individuals with unusual WMH patterns.

*Methods:* Individual participant data (N = 3525, including 777 participants with subjective cognitive decline, 1389 participants with mild cognitive impairment and 1359 patients with dementia) from eleven memory clinic cohorts, recruited through the Meta VCI Map Consortium, were used. WMH segmentations were provided by participating centers or performed in Utrecht and registered to the Montreal Neurological Institute (MNI)-152 brain template for spatial normalization. To determine WMH distribution frequencies, we calculated WMH probability maps at voxel level. To identify individuals with unusual WMH patterns, region-of-interest (ROI) based WMH probability maps, rule-based scores, and a machine learning method (Local Outlier Factor (LOF)), were implemented.

*Results:* WMH occurred in 82% of voxels from the white matter template with large variation between subjects. Only a small proportion of the white matter (1.7%), mainly in the periventricular areas, was affected by WMH in at least 20% of participants. A large portion of the total white matter was affected infrequently. Nevertheless, 93.8% of individual participants had lesions in voxels that were affected in less than 2% of the population, mainly located in subcortical areas. Only the machine learning method effectively identified individuals with unusual patterns, in particular subjects with asymmetric WMH distribution or with WMH at relatively rarely affected locations despite common locations not being affected.

*Discussion:* Aggregating data from several memory clinic cohorts, we provide a detailed 3D map of WMH lesion distribution frequencies, that informs on common as well as rare localizations. The use of data-driven analysis with LOF can be used to identify unusual patterns, which might serve as an alert that rare causes of WMH should be considered.

---

## 1. Introduction

White matter hyperintensities (WMH) are a frequent observation on brain MRI (Wardlaw et al., 2013). The prevalence of WMH is known to increase with age (de Leeuw et al., 2001; Prins and Scheltens, 2015). WMH of presumed vascular origin are primarily due to cerebral small vessel disease (SVD) (Wardlaw et al., 2015), which is the most frequent cause of vascular cognitive impairment and a major contributor to dementia of mixed etiology (Wardlaw et al., 2013). In the context of dementia, WMH, particularly in posterior regions, may also be related to presence of amyloid pathology (Weaver et al., 2019). Clearly, in a broader sense, WMH may be due to many other causes, including inflammation and metabolic disease.

In patients attending a memory clinic, the potential clinical relevance and likely etiology of WMH is often derived from their volume, location, and distribution (Prins and Scheltens, 2015; Biesbroek et al., 2016). Different rating scales have been developed to visually assess the severity of WMH as a proxy for volume in clinical practice, for example the Fazekas (Fazekas et al., 1987) and Scheltens (Scheltens et al., 1993) scales. These scales show a fair correlation with volumetric WMH measures (Kapeller et al., 2003). In contrast, location and distribution are mostly appraised qualitatively, based on expert opinion. The absence

of information about WMH distribution frequencies in memory clinic patients hampers the recognition of specific and possible unusual WMH patterns for an individual patient attending a memory clinic. Such unusual patterns may point to causes that are less common in patients presenting with memory complaints, such as rare monogenic conditions. For example, in Cerebral Autosomal Dominant Arteriopathy with Subcortical Infarcts and Leukoencephalopathy (CADASIL) WMH are commonly seen in the anterior temporal poles and superior frontal gyri whereas these areas are normally spared in SVD (Auer et al., 2001).

With a large international multicenter collaboration of memory clinic studies, we provide detailed and representative data on WMH distribution frequencies in participants attending a memory clinic. Second, we aim to identify individuals with unusual WMH patterns in the dataset. We expected to be able to identify these individuals with rule-based scores based on the derived WMH frequency maps.

## 2. Methods

### 2.1. Participants

We used data from a previous Meta VCI Map Consortium project (Coenen et al., 2023), involving individual participant data from 11 memory clinic cohorts. Meta VCI Map is a consortium that aims to perform *meta*-analyses on strategic lesion locations for vascular cognitive impairment using lesion-symptom mapping (Weaver et al., 2019). Cohorts for the present project were included based on the following criteria: (1) participants were evaluated at an outpatient clinic because of cognitive symptoms; (2) availability of MRI with T1-weighted and either FLAIR or T2-weighted images; (3) availability of neuropsychological data. Participants with any degree of symptom severity (i.e. subjective cognitive decline, mild cognitive impairment, dementia)

could be included and the clinical diagnosis should be compatible with vascular, neurodegenerative or mixed etiology. Participants diagnosed with other causes of cognitive impairment (e.g., excessive alcohol consumption, brain tumor, trauma, multiple sclerosis, psychiatric disorder) or monogenic disorders (e.g., CADASIL, presenilin mutations, or leukodystrophies), were excluded. Central data processing and analysis were performed at the University Medical Center Utrecht (Utrecht, the Netherlands). For all cohorts, ethical and institutional approval were obtained as required by local regulations, including informed consent, to allow data acquisition and data sharing.

The dataset for the current study was previously used to examine the cognitive impact of WMH in individuals attending a memory clinic (Coenen et al., 2023). Therefore, only participants with available neuropsychological data were included, however the neuropsychological data were not used for the current analyses.

Background and organization of the Meta VCI Map consortium is described in the design paper (Weaver et al., 2019) and on the consortium website (https://metavcimap.org). A flowchart of participant selection is provided in Figure A.1. Details on MRI scan protocols per cohort are described in the supplements.

## 2.2. Image processing and analysis

Binary WMH segmentations were provided by the participating centers or automatically computed (Kuijf et al., 2019) at the UMC Utrecht, the Netherlands. FLAIR images were used for WMH segmentation in ten cohorts; in one cohort (YOAD), WMH were segmented on T2-weighted images. More details on WMH segmentation methods are described in the supplementary material.

All analyses were performed in a standard space rather than native space. To this end, WMH segmentations were registered to the $1 \times 1 \times 1$ mm resolution Montreal Neurological Institute (MNI)-152 brain template for spatial normalization (Fonov et al., 2011) (see supplementary material for further details). Two cohorts (AUCD, ADNI) shared WMH segmentations that were already registered to MNI space. For the remaining cohorts, WMH segmentations were registered to the MNI template centrally using RegLSM (Biesbroek et al., 2019). First, the FLAIR or T2-weighted images were registered to the corresponding native T1 image with a linear registration. Second, the T1 image was subsequently transformed to the T1 1-mm MNI-152 template, using a linear registration followed by a non-linear registration. An age-specific MRI template (Fonov et al., 2011) was used as an intermediate step before the final registration to MNI-152 space in order to improve the quality of the results by providing a better match between participant and template. These transformations were combined into a single transformation that was used as a final step to transform the corresponding WMH segmentation to the MNI-152 template. All registration results were visually inspected to ensure that the procedure was successful. Failed registrations were excluded (in total 2.7 % of participants, see Figure A.1).

Voxels located outside the white matter (defined using the MNI probabilistic white matter atlas (Fonov et al., 2009), threshold at 30 %) were removed from all individual WMH segmentations to minimize the effect of possible misclassifications.

For quality control, a random subset of ten WMH maps was returned to each participating center where they were asked to check whether the registered WMH map properly represented the WMH segmentation on the original FLAIR/T2-weigthed images. This quality control step revealed no data handling or processing errors. More details on WMH segmentation, registration procedures, and quality checks were described previously (Coenen et al., 2023).

## 2.3. WMH probability maps

The binary WMH segmentations were registered to the MNI-152 template (see Section 2.2). In this template space, all transformed binary WMH segmentations were summed and next divided by the total number of participants. This resulted in a WMH probability map at the voxel level, indicating the probability of a voxel containing a WMH lesion or not. In addition, to better visualize WMH distributions according to WMH burden, three probability maps including participants with low / medium / high tertiles of normalized WMH volume were created. In the supplements, cutoff values show voxels affected in less than 0.1 %, 0.5 %, and 2.0 % of the participants, to visualize at which locations of the brain voxels are rarely affected.

## 2.4. Detection of unusual patterns

To identify unusual WMH patterns based on differential burden in different tracts, WMH probability maps at a region-of-interest (ROI) level were created using the JHU-atlas (threshold at 10 % (Hua et al., 2008). This atlas considers twenty major white matter tracts.

Additionally, two rule-based scores and a machine learning-based score were explored. The first rule-based score (RB Score 1) was derived from WMH distribution frequencies, assigning a high score to participants having WMH voxels in low-probability regions based on the probability distribution of the whole cohort. It was calculated as 1 – the probability of a lesion in a certain voxel, and this was summed up for all voxels. The score was individually adjusted for total normalized WMH volume, by dividing the score with the square root of the total normalized WMH volume per participant.

The second rule-based score (RB Score 2) assigned a high score to lesions (of at least ten voxels in size) at locations where less than five participants had a lesion. It was implemented by assessing only lesions at locations where less than five participants in the dataset had a lesion by masking out all other locations, and computing the sum of 1 – the probability of a lesion in a certain voxel for all remaining voxels. The score was individually adjusted for total normalized WMH volume, by dividing the score with the square root of the total normalized WMH volume per participant.

The machine learning-based score used Local Outlier Factor (LOF) (Breunig et al., 2000), an unsupervised anomaly detection method. LOF considers the full 3D distribution of WMH voxels of each participant, whereas the rule-based scores mainly consider individual or regionally clustered voxel locations. LOF assigns a low (negative) score to participants whose total 3D WMH distribution deviates substantially with respect to all other participants in the dataset.

We assumed that a score which was strongly correlated to normalized WMH volume, was not suitable in the detection of unusual patterns. This would mostly identify participants with a high total WMH volume as outliers, whereas rare spatial distribution patterns may be related to location instead of volume.

## 2.5. Statistical analyses

Baseline characteristics were calculated using IBM SPSS Statistics 26.0.0.1. The resulting WMH probability map is published on DataverseNL (https://doi.org/10.34894/FYL9ID). The correlation between RB score 1, 2, and LOF with total normalized WMH volume was calculated using Pearson correlation in SciPy.

The implementation of RB score 1, 2, and LOF was published on GitHub (https://github.com/Meta-VCI-Map/WMH_distribution_memory_clinic).

## 3. Results

### 3.1. Participants

The total study sample consisted of 3525 participants (49.9 % female) from 11 memory clinic cohorts. Mean age was 71.6 years (SD 9.0 years). A total of 777 participants (22.0 %) had subjective cognitive decline (SCD), 1389 participants (39.4 %) had mild cognitive

impairment (MCI), and 1359 patients (38.6 %) had dementia. Of those with dementia 804 patients (59.2 %) were diagnosed with Alzheimer's disease, 85 patients (6.3 %) with vascular dementia, 44 patients (3.2 %) with frontotemporal dementia, 24 patients (1.8 %) with Lewy body dementia, and 59 patients (4.3 %) with dementia with other etiology. For the remaining 343 patients (25.2 %) with dementia the etiology was unknown or not available in the database. Median normalized WMH volume was 6.1 ml (IQR 2.2–16.3 ml). Table 1 shows the participant characteristics according to WMH tertile.

### 3.2. WMH probability maps

Voxel wise WMH probability maps of WMH distribution for the whole cohort are shown in Fig. 1 and for the three WMH tertiles in Fig. 2. In total, WMH locations involved 82 % of the white matter.

#### 3.2.1. Commonly affected locations

Despite the observation that 82 % of the white matter could be affected by WMH, only few locations were affected in a substantial subset of participants. For example, only 1.7 % of the white matter was affected in at least 20 % of participants, 4.6 % in at least 10 %, and 9.9 % in at least 5 %. The periventricular areas—including frontal, occipital, and parietal—were most commonly affected (Fig. 1; shown in red). This was consistently observed in all three WMH tertiles (Fig. 2). The centrum semiovale and corona radiata were relatively commonly affected by WMH in all three tertiles, but the overall probability increased with total normalized WMH volume.

#### 3.2.2. Moderately frequent affected locations

Subcortical areas, just outside the periventricular areas commonly referred to as "deep", were affected by WMH with moderate frequency and more often affected in the medium and high WMH tertiles (Fig. 2). The frontal, occipital, and parietal areas were equally affected, with increasing probability as total normalized WMH volume increases. The temporal lobe was less frequently affected, compared to these other lobes; and rarely affected in the low and medium WMH tertiles.

#### 3.2.3. Rarely affected locations

A large part of the white matter was rarely affected. For example, 68.3 % was affected in less than 0.1 % of participants, 30.4 % in less



**Fig. 1.** WMH probability map at the voxel level for the whole cohort. This figure shows the spatial probability distribution of WMH overlaid onto the MNI-152 template. Colors indicate the percentage of participants who have a WMH in a given voxel. L = left, R = right.

1.0 %, and 20.8 % in less than 2.0 %. All rarely affected WMH locations were widespread throughout the white matter (Fig. 1; shown in yellow). Even in the low WMH tertile, WMH could be present dispersed across rarely affected locations. The infratentorial regions were more rarely affected compared to the supratentorial white matter. When the infratentorial white matter was affected, WMH were mostly located in the pons. The basofrontal white matter and the temporal lobes were rarely affected by WMH, especially in the low and medium WMH tertiles. The internal capsule was also rarely affected, but in higher WMH tertiles WMH were sometimes present more cranially and in the anterior limb. Compared to the internal capsule, the external capsule was relatively more often affected in the medium and high WMH tertiles.

In the genu of the corpus callosum, WMH were almost never observed in any of the WMH tertiles. The body of the corpus callosum was hardly affected in the low / medium WMH tertiles and only sometimes in the high WMH tertile. This also held for the splenium, except that the septum pellucidum (at the splenium / CSF boundary) can appear hyperintense on FLAIR or T2 imaging and is sometimes classified as WMH. In Fig. 3, the corpus callosum is part of multiple tracts. Given that the corpus callosum itself was rarely affected, the occurrence of WMH in these tracts was thus caused by the lateral extensions of each tract.

The grey matter in the basal ganglia contained some WMH for participants in the high WMH tertile. This is likely owing to the partial volume effect—where a single voxel can contain both gray and white matter—in combination with the used threshold of 30 % for the presence of white matter in individual voxels of the MNI probabilistic atlas. In addition, this might also be partially attributed to technicalities, such as errors in the automatic segmentation or misregistration.

Eighteen% of the white mater was not affected by WMH in any of the participants, which mostly include juxtacortical white matter.

### 3.3. Detection of unusual patterns

Figure A.2 shows that 2387 participants (67.7 %) had a lesion-containing voxel at a location where the overall lesion prevalence was < 0.1 %, 3018 participants (85.6 %) had a lesion-containing voxel at a location where the overall lesion prevalence was < 0.5 %, and 3305 participants (93.8 %) had a lesion-containing voxel at a location where the overall lesion prevalence was < 2.0 %. In other words: the vast

**Table 1**
Participant characteristics and WMH features according to voxel based WMH distribution.

| Characteristics | Normalized WMH volume | | |
| --- | --- | --- | --- |
| | Low | Medium | High |
| Number of participants | 1175 | 1175 | 1175 |
| Age (years), mean (SD) | 67.9 (8.8) | 72.0 (8.4) | 74.8 (8.6) |
| Female, n (%) | 605 (51.5) | 557 (47.4) | 597 (50.8) |
| Diagnosis, n (%) | | | |
| SCD | 402 (34.2) | 222 (18.9) | 153 (13.0) |
| MCI | 490 (41.7) | 463 (39.4) | 364 (37.1) |
| Dementia | 283 (24.1) | 490 (41.7) | 586 (49.9) |
| Dementia, n (%)$^\$$ | | | |
| AD | 145 (51.2) | 290 (59.2) | 369 (63.0) |
| VaD | 1 (0.4) | 11 (2.2) | 73 (12.5) |
| LBD | 5 (1.8) | 13 (2.6) | 6 (1.0) |
| FTD | 14 (4.9) | 18 (3.7) | 12 (2.0) |
| Dementia with other etiology | 13 (4.6) | 18 (3.7) | 28 (4.7) |
| MMSE, mean (SD) | 26.5 (4.1)$^\#$ | 24.7 (4.6)$^\#$ | 23.9 (5.0)$^\#$ |
| Normalized WMH volume (ml), range | 0.0 – 3.2 | 3.2 – 11.4 | 11.4 – 202.8 |
| BPF, median (IQR) | 0.7 (0.1)$^\$$ | 0.7 (0.1)$^\#$ | 0.7 (0.1)$^\#$ |

Characteristics are presented per normalized WMH tertile. A WMH lesion was defined as 10 neighboring affected voxels. *missing in < 1 %, # missing in 1–10 %, $ missing in > 10 %. SCD: Subjective Cognitive Decline, MCI: Mild Cognitive Impairment, AD: Alzheimer's disease, VaD: Vascular Dementia, LBD: Lewy body dementia, FTD: Frontotemporal dementia, MMSE: Mini Mental State Examination, BPF: brain parenchymal fraction.
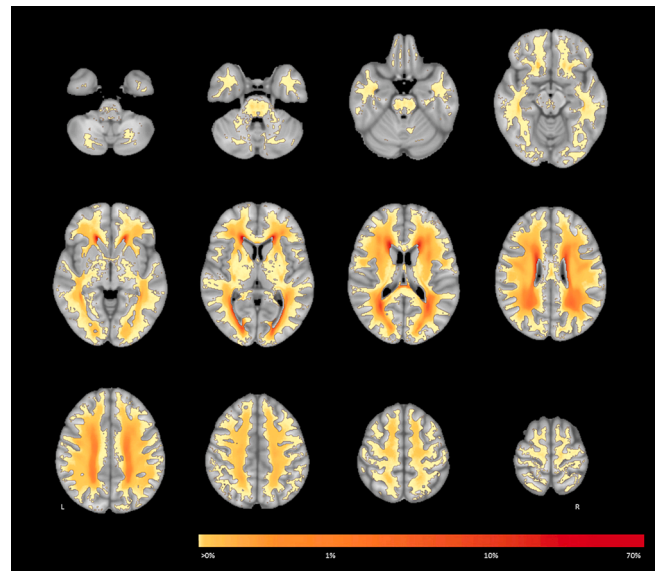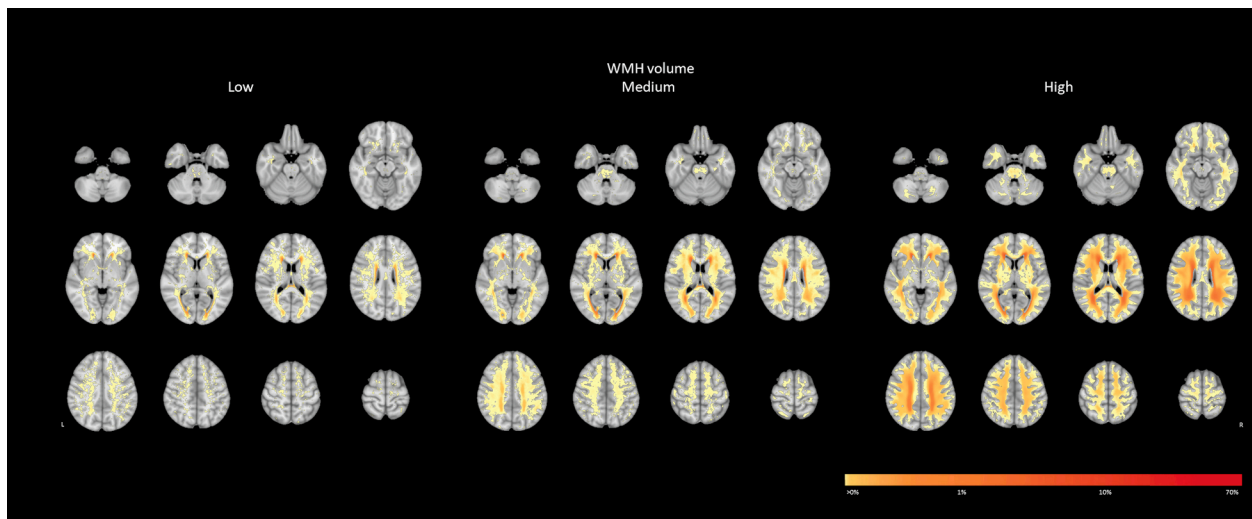
**Fig. 2.** WMH probability map at the voxel level stratified by WMH tertile. This figure shows the spatial probability distribution of WMH overlaid onto the MNI-152 template per WMH tertile. Colors indicate the percentage of participants who have a WMH in a voxel in that tertile. L = left, R = right.
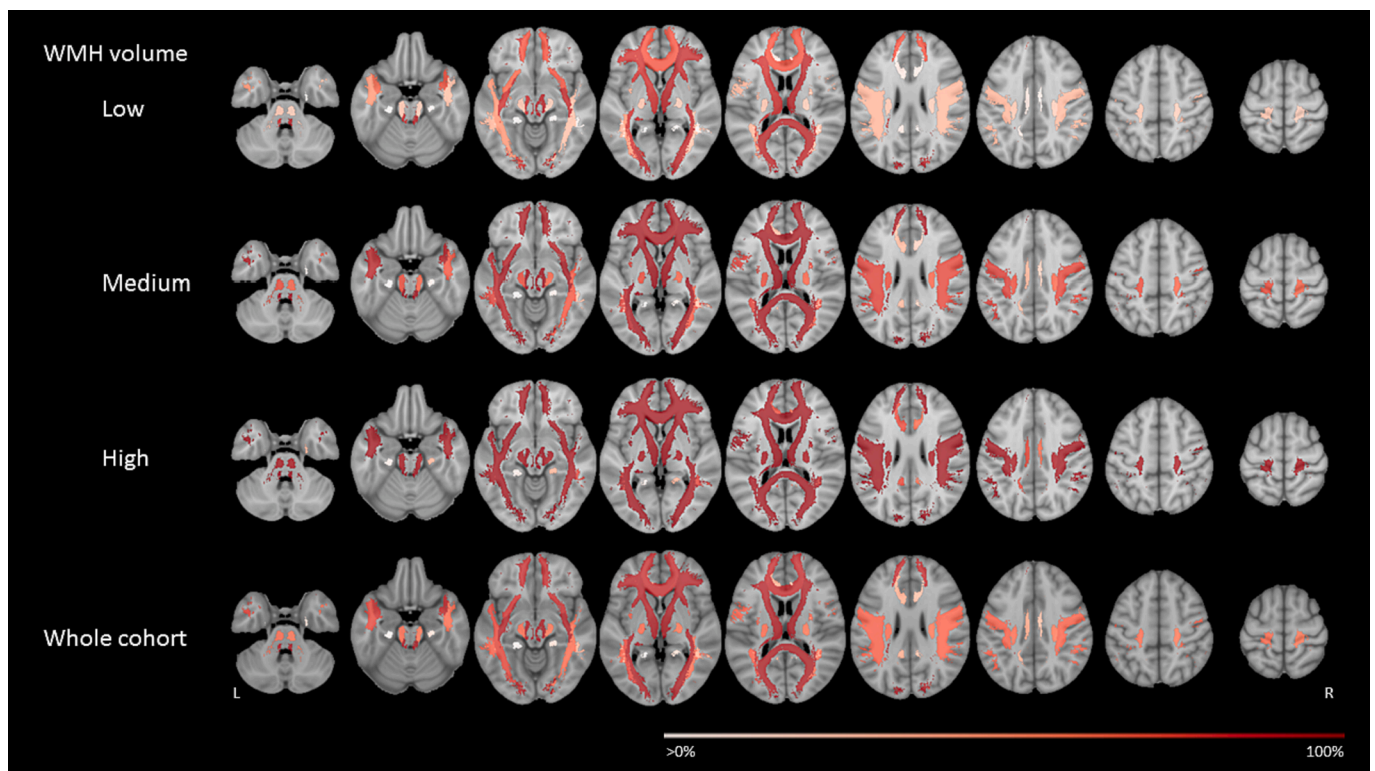


**Fig. 3.** Region-of-interest based WMH probability map. This figure shows the region-of-interest based WMH spatial probability distribution for the whole cohort and per normalized WMH tertile. Regions-of-interest are defined according to twenty major white matter tracts defined in the JHU atlas (probability threshold of 10 %) (Hua et al., 2008). Colors indicate the percentage of participants who have a WMH (partially) overlapping with that region-of-interest. L = left, R = right.

majority of participants had lesions at locations that might be considered unusual just based on lesion frequency alone.

Consistent with the voxel-based results, WMH probability maps at tract-based ROI level (Fig. 3) showed that in the periventricular tracts (anterior thalamic radiation left and right, and the forceps major), the occurrence of WMH was slightly higher than in the other tracts. This was best observed in the low WMH tertile. Fig. 3 also showed that the probability for occurrence of WMH was low in the cingulum and cingulate gyrus, across all three WMH tertiles. However, differences in probabilities between tracts were small (Table A.1). We therefore

concluded that a tract-based ROI approach did not help to identify unusual patterns.

Results of RB Score 1 were essentially collinear with normalized WMH volume (R = 0.99, P = 0.0), also after individualized WMH volume adjustment, i.e. the score that included the square root of the total normalized WMH volume (R = 0.96, P = 0.0). This score was therefore deemed unsuitable to identify individuals with unusual patterns and no further analyses were performed. This is in line with the findings in Figure A.2, which show that almost all participants in our pooled cohort had WMH at a location that is rarely affected in the total study sample.

Results of RB Score 2 were moderately correlated with normalized WMH volume (R = 0.48, P < 0.0001), also after individualized WMH volume adjustment, i.e. the score that included the square root of the total normalized WMH volume (R = 0.32, P < 0.0001). Participant characteristics, including age, sex, and diagnosis, and WMH segmentations in native space were assessed for twenty participants with the most extreme scores (highest values) for Score 2. Visual inspection of the results revealed that Score 2 mostly detected WMH patterns with WMH at common locations. Score 2 also identified WMH patterns from participants with a high normalized WMH volume. Therefore, Score 2 does not seem an appropriate method in the detecting unusual patterns. Score 2 also identified some errors made by the automatic WMH segmentation in 12 out of 20 participants, including acute or chronic infarcts segmented as WMH. Fig. 4 shows the five most unusual WMH patterns for Score 2, after exclusion of segmentation errors.

Results of the LOF were weakly correlated with normalized WMH volume (R = 0.24, P < 0.0001). The results from LOF were assessed by examining the participant characteristics and WMH segmentation in native space for twenty patients with the most extreme scores (i.e. lowest values). Visual inspection of the WMH segmentations showed asymmetric patterns and absence of WMH at common locations. Besides this, LOF also revealed errors made by the automatic WMH segmentation in 10 out of 20 participants. Fig. 5 shows the participant characteristics and WMH segmentations of the five most unusual WMH patterns, after exclusion of segmentation errors.

As a reference, to check whether segmentation errors were a specific finding of LOF or reflected a more common occurrence of segmentation errors in the study sample, a random sample of 60 participants from the whole dataset was rechecked. This sample revealed no segmentation errors.

## 4. Discussion

This study provides a detailed 3D map of WMH lesion distribution frequencies in a large multicenter memory clinic cohort. Due to the large sample size, we were able to identify commonly, moderately frequent, and rarely affected lesion locations. Additionally, LOF was able to identify unusual WMH distribution patterns. These unusual patterns included asymmetric WMH patterns and WMH presence at rare locations in the absence of WMH at common locations. This work can be used to compare against published WMH distribution maps of other neurodegenerative disease groups (Dadar et al., 2022) or aid clinical research studies (Botz et al., 2023).

Voxel wise WMH probability maps (Figs. 1 & 2) showed that WMH distribution frequencies are highly variable and that it is common to have WMH at unusual locations: e.g. 93.8 % of participants had at least one lesion-containing voxel at a location that was affected in less than 2 % of individuals (Figure A.2). Of note, 18 % of the white matter was not affected by WMH in any of the participants, indicating that the probability of WMH to occur in these voxels is below 0.03 %. The periventricular areas were most commonly affected. Rarely affected locations were widespread throughout the white matter. Since many participants had lesions at locations that might be considered as unusual based on lesion frequency alone, the total distribution pattern should be considered when assessing unusual distribution patterns on the level of an individual participant. Our results are in line with previous smaller studies on WMH distribution in a memory clinic setting, indicating that periventricular lesions are common (Prins and Scheltens, 2015; Yoshita et al., 2006; Holland et al., 2008), and the infratentorial regions and the corpus callosum are rarely affected (Yoshita et al., 2006; Barkhof and Scheltens, 2002). Another study including community-based individuals
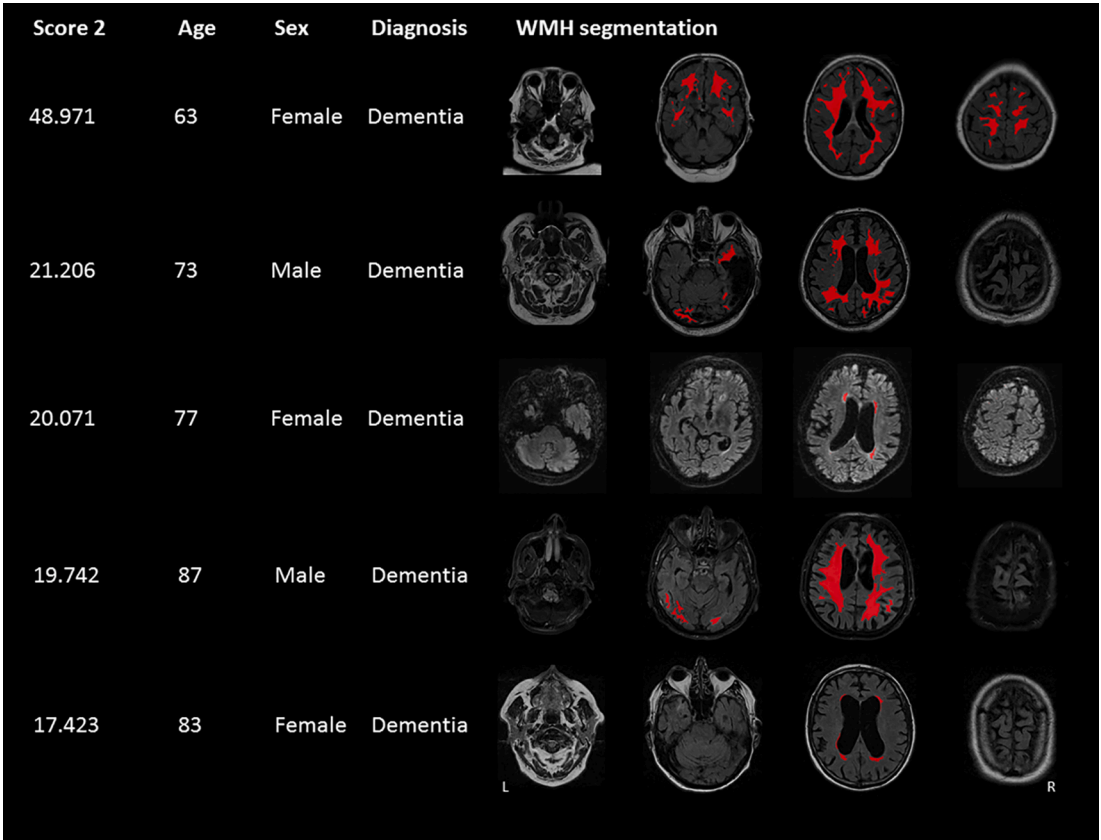
| Score 2 | Age | Sex | Diagnosis | WMH segmentation |
|---|---|---|---|---|
| 48.971 | 63 | Female | Dementia | |
| 21.206 | 73 | Male | Dementia | |
| 20.071 | 77 | Female | Dementia | |
| 19.742 | 87 | Male | Dementia | |
| 17.423 | 83 | Female | Dementia | |

**Fig. 4.** Results of Rule based Score 2. Clinical characteristics and WMH distribution patterns of the five participants with the highest Score 2 are presented, after exclusion of segmentations errors. Score 2 assigns a high score to lesions (of at least ten voxels in size) at locations where less than five participants had a lesion and this score was calculated by computing the sum of 1 – probability of a lesion in a certain voxel for these locations. The FLAIR sequence and WMH lesion map in native space are shown. L = left, R = right.
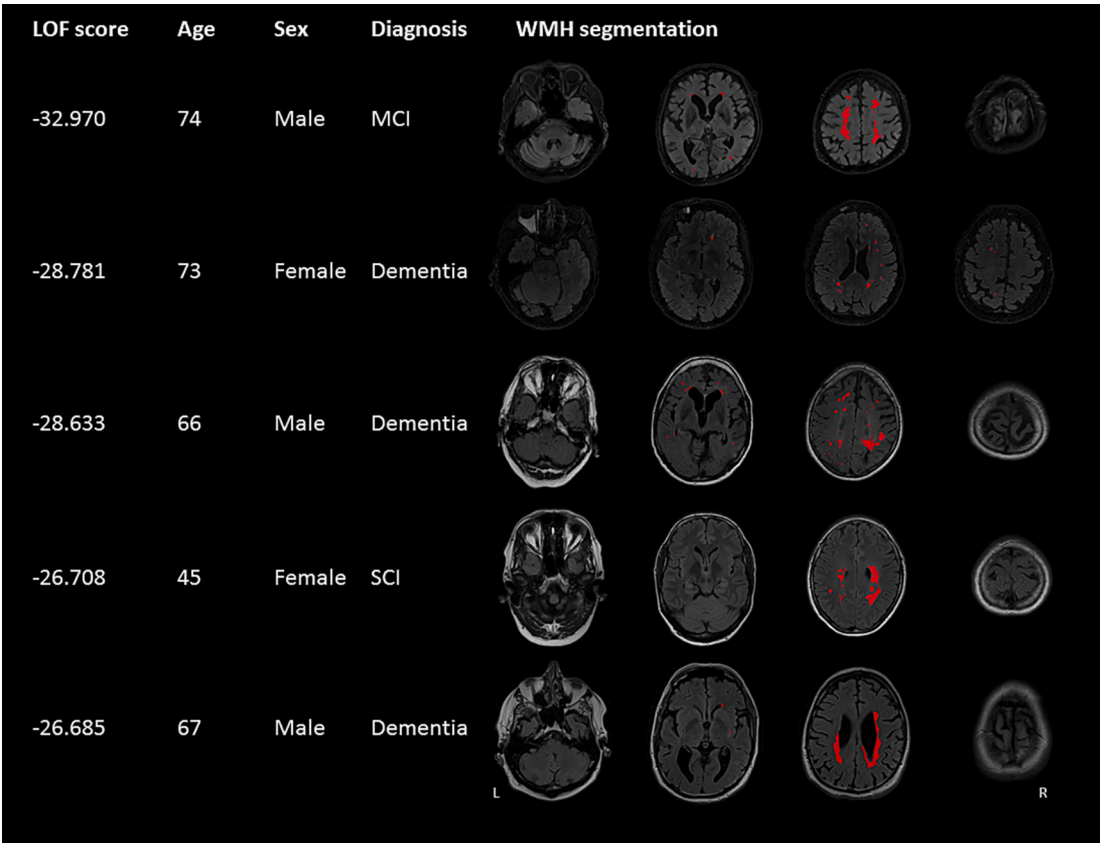
**Fig. 5.** Results of local outlier factor. Clinical characteristics and WMH distribution patterns of the five participants with the lowest local outlier factor (LOF) score are presented, after exclusion of segmentations errors. LOF assigns a low (negative) score to participants whose total 3D WMH distribution deviates substantially with respect to all other participants in the dataset. The FLAIR sequence and WMH lesion map in native space are shown. L = left, R = right.

also showed that with increasing WMH volume, WMH were expanded to more subcortical areas (DeCarli et al., 2005). In this study, we performed all WMH distribution analyses in the MNI-152 template space. An inherent consequence of image registration (which enables analyses of WMH distribution and volume across participants and corrects for differences in brain size) is possible changes in WMH volume, but the relative spatial distribution remains intact. Since the primary focus of this study was WMH distribution frequencies, any possible volume changes owing to registration would not influence our conclusions drawn from the WMH distribution frequencies.

ROI based WMH probability maps, considering twenty major white matter tracts, showed that differences in probabilities between tracts were small and therefore this approach seemed not very informative in detecting unusual WMH patterns. Using two rule-based scores to identify unusual WMH patterns proved also unsuccessful, mainly identifying participants with a high total normalized WMH volume or distribution patterns with WMH at common locations. A data-driven machine learning approach, using the anomaly detection method LOF, did prove successful in identifying unusual WMH patterns, which included individuals with asymmetric patterns or the absence of WMH at common locations.

Our study has several strengths. To our knowledge, this is the largest study presenting and analyzing a 3D voxel wise WMH distribution map in a memory clinic setting. By including data from eleven memory clinic cohorts, we were able to create a WMH distribution map that almost covers the full white matter. The WMH distribution maps on the voxel level provide a high spatial resolution and allows for quantitative visualization and analysis of the heterogeneity of WMH distributions. The use of our previously published and validated image analysis workflow (Biesbroek et al., 2019) creates uniform output for all cohorts included in our study, enabling the analysis of multicenter data with

different MRI scanners and acquisition protocols. This also enabled post-hoc pooling of multicenter data of a heterogeneous population, improving generalizability to a memory clinic setting.

However, several potential limitations of the study should be noted. Participating cohorts had different inclusion criteria and therefore our study sample may not be exactly representative to a general memory clinic population. In particular, different cohorts used different standardized diagnostic criteria for SCD, MCI, and dementia which may have caused heterogeneity in terms of diagnostic groups. Of note, we only included participants where the clinical diagnosis was compatible with vascular, neurodegenerative or mixed etiology, likely also including participants without major pathology. Participants with other diagnoses, which may have been based on aberrant patterns of WMH, were excluded by design. Hence, the findings of our study primarily apply to the selected patient categories. However, it should also be noted that from 343 patients with dementia (25 %) the etiology was unknown or not available in the database. It can therefore not be ruled out that these patients meet one of the exclusion criteria. As expected, the clinical characteristics of participants in the three WMH tertiles are slightly different (e.g. age, diagnosis), which should be taken into account when comparing WMH distribution frequencies across these groups. Different cohorts used different scan protocols and different resolution, although all scans where registered to the same standard space this will have affected the granularity of the results. Moreover, one cohort, including 994 (28.2 %) participants had missing segmentations of the infratentorial region. Hence, the WMH probability of < 0.1 % in the majority of infratentorial regions and < 0.5 % in the central pons (Figure A.2), may be a slight underestimation. Results of the ROI-based analyses are limited by the spatial coverage of the JHU atlas, which only covers approximately 40 % of the total white matter (despite using a low probability threshold). Besides unusual patterns, LOF also revealed

errors made earlier during the automatic segmentation of WMH, where acute or chronic infarcts were incorrectly segmented as WMH. Such errors are to be expected in a study with this sample size. In a post-hoc random quality controls sample of 60 scans no such errors were identified. Hence, LOF could also be used as a computer-assisted quality control for large studies using WMH segmentations to detect segmentation errors. Finally, other aspects of lesions, such as shape, may be considered to identify abnormal patterns. Here we primarily addressed spatial distribution.

Future work could repeat distribution analyses in other settings, such as community-based cohorts; to provide complimentary information to the results presented here. In the current study it was not possible to assess to which extent the observed WMH pattern is because of disease processes related to cognitive impairment or normal aging. A previous study by Wollenweber *et al.* (2017) (Wollenweber et al., 2017) compared the spatial distribution of different SVD imaging markers between community-based participants and patients with CADASIL and cerebral amyloid angiopathy (CAA). However, that study was limited in terms of sample size and different etiologies.

In clinical research or routine LOF might serve as an alert to notify observers about unusual patterns to which extra attention should be paid and other causes than sporadic SVD or amyloid pathology could be considered. Future studies should examine to which extent lesion distributions provide diagnostic or prognostic information, or help to recognize specific etiologies. For example, WMH distribution maps per diagnostic group (i.e. SCD, MCI, and dementia) using standardized diagnostic criteria could be addressed. Second, a semi-automated technique, like LOF, may be helpful in identifying WMH in a multispot pattern which is part of the Boston 2.0 criteria (Charidimou et al., 2022) for CAA and which is now currently based on visual review. This is a field which is rapidly evolving, benefiting from developments in machine learning and artificial intelligence.

In summary, this study provides a quantitative WMH distribution map in a large multicenter memory clinic cohort. Many participants proved to have at least some WMH at a location where WMH occurred infrequently. Identifying unusual WMH patterns is therefore not straightforward on visual evaluation or rule-based schemes alone, but can be achieved by an automatic machine learning method. This knowledge may be helpful to researchers and clinicians in assessing WMH distribution and identifying unusual patterns which might be associated with other causes than sporadic SVD.

## CRediT authorship contribution statement

**Mirthe Coenen:** Conceptualization, Data curation, Formal analysis, Investigation, Methodology, Project administration, Visualization, Writing – original draft, Writing – review & editing. **Geert Jan Biessels:** Conceptualization, Data curation, Funding acquisition, Investigation, Methodology, Supervision, Writing – original draft, Writing – review & editing. **Charles DeCarli:** Investigation, Writing – original draft. **Evan F. Fletcher:** Investigation. **Pauline M. Maillard:** Investigation. **Frederik Barkhof:** Investigation. **Josephine Barnes:** Investigation, Writing – original draft. **Thomas Benke:** Investigation, Writing – original draft. **Jooske M.F. Boomsma:** Investigation. **Christopher P.L.H. Chen:** Investigation, Writing – original draft. **Peter Dal-Bianco:** Investigation, Investigation, Writing – original draft. **Anna Dewenter:** Investigation, Writing – original draft. **Marco Duering:** Investigation, Formal analysis, Writing – original draft. **Christian Enzinger:** Investigation, Writing – original draft. **Michael Ewers:** Investigation, Writing – original draft. **Lieza G. Exalto:** Investigation, Writing – original draft. **Nicolai Franzmeier:** Investigation, Writing – original draft. **Onno Groeneveld:** Investigation. **Saima Hilal:** Investigation. **Edith Hofer:** Investigation. **Huiberdina L. Koek:** Investigation, Writing – original draft. **Andrea B. Maier:** Investigation. **Cheryl R. McCreary:** Investigation. **Janne M. Papma:** Investigation. **Ross W. Paterson:** Investigation, Writing – original draft. **Yolande A.L. Pijnenburg:** Investigation. **Anna Rubinski:** Investigation, Writing – original draft. **Reinhold Schmidt:** Investigation, Writing – original draft. **Jonathan M. Schott:** Investigation, Writing – original draft. **Catherine F. Slattery:** Investigation, Writing – original draft. **Eric E. Smith:** Investigation, Writing – original draft. **Carole H. Sudre:** Investigation. **Rebecca M.E. Steketee:** Investigation. **Esther van den Berg:** Investigation. **Wiesje M. van der Flier:** Investigation, Writing – original draft. **Narayanaswamy Venketasubramanian:** Investigation. **Meike W. Vernooij:** Investigation. **Frank J. Wolters:** Investigation, Formal analysis, Writing – original draft. **Xu Xin:** Investigation. **J. Matthijs Biesbroek:** Conceptualization, Data curation, Funding acquisition, Investigation, Methodology, Supervision, Writing – original draft, Writing – review & editing. **Hugo J. Kuijf:** Conceptualization, Formal analysis, Investigation, Methodology, Software, Supervision, Validation, Visualization, Writing – original draft, Writing – review & editing.

## Declaration of competing interest

The authors declare the following financial interests/personal relationships which may be considered as potential competing interests: FB is supported by the NIHR biomedical research center at UCLH. MD received honoraria for lectures from Bayer Vital and Sanofi Genzyme, Consultant for Hovid Berhad and Roche Pharma. RWP received honoraria from GE Healthcare and is co-lead of Neurofilament light consortium. CHS is supported by an Alzheimer's Society Fellowship. The remaining authors have nothing to disclose.

## Data availability

The WMH probability map is published on DataverseNL (link available in manuscript). The implementation of RB Score 1, 2, and LOF was published on GitHub (link available in manuscript).

## Acknowledgements

We are grateful to the diverse participants who contribute to our research.

## Appendix A. Supplementary data

Supplementary data to this article can be found online at https://doi.org/10.1016/j.nicl.2023.103547.

## References

Auer DP, Pütz B, Gössl C, Elbel GK, Gasser T, Dichgans M. Differential Lesion Patterns in CADASIL and Sporadic Subcortical Arteriosclerotic Encephalopathy: MR Imaging Study with Statistical Parametric Group Comparison. Vol 218.; 2001.

Barkhof, F., Scheltens, P., 2002. Imaging of white matter lesions. Cerebrovasc Dis. 13 (suppl 2), 21–30.

Biesbroek, J.M., Weaver, N.A., Hilal, S., et al., 2016. Impact of strategically located white matter hyperintensities on cognition in memory clinic patients with small vessel disease. PLoS One 11 (11). https://doi.org/10.1371/journal.pone.0166261.

Biesbroek, J.M., Kuijf, H.J., Weaver, N.A., Zhao, L., Duering, M., Biessels, G.J., 2019. Brain infarct segmentation and registration on MRI or CT for lesion-symptom mapping. J. Vis. Exp. 2019 (151) https://doi.org/10.3791/59653.

Botz, J., Lohner, V., Schirmer, M.D., 2023. Spatial patterns of white matter hyperintensities: a systematic review. Front Aging Neurosci. 15. https://doi.org/10.3389/fnagi.2023.1165324.

Breunig, M.M., Kriegel, H.P., Ng, R.T., Sander, J.L.O.F., 2000. ACM SIGMOD Rec. 29 (2), 93–104. https://doi.org/10.1145/335191.335388.

Charidimou, A., Boulouis, G., Frosch, M.P., et al., 2022. The Boston criteria version 2.0 for cerebral amyloid angiopathy: a multicentre, retrospective, MRI–neuropathology diagnostic accuracy study. Lancet Neurol. 21 (8), 714–725. https://doi.org/10.1016/S1474-4422(22)00208-3.

Coenen, M., Kuijf, H.J., Huenges Wajer, I.M.C., et al., 2023. Strategic white matter hyperintensity locations for cognitive impairment: A multicenter lesion-symptom mapping study in 3525 memory clinic patients. Alzheimer's & Dementia. 19, 2420–2432. https://doi.org/10.1002/alz.12827.

Dadar, M., Mahmoud, S., Zhernovaia, M., Camicioli, R., Maranzano, J., Duchesne, S., 2022. White matter hyperintensity distribution differences in aging and neurodegenerative disease cohorts. Neuroimage Clin. 36, 103204 https://doi.org/10.1016/j.nicl.2022.103204.

de Leeuw, F.E., de Groot, J.C., Achten, E., et al., 2001. Prevalence of cerebral white matter lesions in elderly people: A population based magnetic resonance imaging study. The Rotterdam Scan Study. J Neurol Neurosurg Psychiatry. 70 (1), 9–14. https://doi.org/10.1136/jnnp.70.1.9.

DeCarli, C., Fletcher, E., Ramey, V., Harvey, D., Jagust, W.J., 2005. Anatomical mapping of white matter hyperintensities (WMH): Exploring the relationships between periventricular WMH, deep WMH, and total WMH burden. Stroke 36 (1), 50–55. https://doi.org/10.1161/01.STR.0000150668.58689.f2.

Fazekas, F., Chawluk, J.B., Alavi, A., 1987. MR signal abnormalities at 1.5 T in Alzheimer's dementia and normal aging. Am. J. Neuroradiol. 8 (3), 421–426.

Fonov, V., Evans, A., McKinstry, R., Almli, C., Collins, D., 2009. Unbiased nonlinear average age-appropriate brain templates from birth to adulthood. Neuroimage 47, S102. https://doi.org/10.1016/S1053-8119(09)70884-5.

Fonov, V., Evans, A.C., Botteron, K., Almli, C.R., McKinstry, R.C., Collins, D.L., 2011. Unbiased average age-appropriate atlases for pediatric studies. Neuroimage 54 (1), 313–327. https://doi.org/10.1016/j.neuroimage.2010.07.033.

Holland, C.M., Smith, E.E., Csapo, I., et al., 2008. Spatial distribution of white-matter hyperintensities in Alzheimer disease, cerebral amyloid angiopathy, and healthy aging. Stroke 39 (4), 1127–1133. https://doi.org/10.1161/STROKEAHA.107.497438.

Hua, K., Zhang, J., Wakana, S., et al., 2008. Tract probability maps in stereotaxic spaces: Analyses of white matter anatomy and tract-specific quantification. Neuroimage 39 (1), 336–347. https://doi.org/10.1016/j.neuroimage.2007.07.053.

Kapeller, P., Barber, R., Vermeulen, R.J., et al., 2003. Visual Rating of Age-Related White Matter Changes on Magnetic Resonance Imaging. Stroke 34 (2), 441–445. https://doi.org/10.1161/01.STR.0000049766.26453.E9.

Kuijf, H.J., Casamitjana, A., Collins, D.L., et al., 2019. Standardized Assessment of Automatic Segmentation of White Matter Hyperintensities and Results of the WMH Segmentation Challenge. IEEE Trans Med Imaging. 38 (11), 2556–2568. https://doi.org/10.1109/TMI.2019.2905770.

Prins, N.D., Scheltens, P., 2015. White matter hyperintensities, cognitive impairment and dementia: An update. Nat Rev Neurol. 11 (3), 157–165. https://doi.org/10.1038/nrneurol.2015.10.

Scheltens, P., Barkhof, F., Leys, D., et al., 1993. A semiquantitative rating scale for the assessment of signal hyperintensities on magnetic resonance imaging. J Neurol Sci. 114 (1), 7–12. https://doi.org/10.1016/0022-510X(93)90041-V.

Wardlaw, J.M., Smith, E.E., Biessels, G.J., et al., 2013. Neuroimaging standards for research into small vessel disease and its contribution to ageing and neurodegeneration. Lancet Neurol. 12 (8), 822–838. https://doi.org/10.1016/S1474-4422(13)70124-8.

Wardlaw, J.M., Valdés Hernández, M.C., Muñoz-Maniega, S., 2015. What are white matter hyperintensities made of? J Am Heart Assoc. 4 (6) https://doi.org/10.1161/JAHA.114.001140.

Weaver, N.A., Zhao, L., Biesbroek, J.M., et al., 2019. The Meta VCI Map consortium for meta-analyses on strategic lesion locations for vascular cognitive impairment using lesion-symptom mapping: Design and multicenter pilot study. Alzheimer's Dementia: Diag. Assess. Disease Monitor. 11, 310–326. https://doi.org/10.1016/j.dadm.2019.02.007.

Weaver, N.A., Doeven, T., Barkhof, F., et al., 2019. Cerebral amyloid burden is associated with white matter hyperintensity location in specific posterior white matter regions. Neurobiol Aging. 84, 225–234. https://doi.org/10.1016/j.neurobiolaging.2019.08.001.

Wollenweber, F.A., Baykara, E., Zedde, M., et al., 2017. Cortical superficial siderosis in different types of cerebral small vessel disease. Stroke 48 (5), 1404–1407. https://doi.org/10.1161/STROKEAHA.117.016833.

Yoshita, M., Fletcher, E., Harvey, D., et al., 2006. Extent and distribution of white matter hyperintensities in normal aging, MCI, and AD. Neurology 67, 2192–2198.